



Applying the passive energy balancing concept into the actuation system of a morphing rotorcraft: integration and optimisation

C. Wang¹, J. Zhang², A.D. Shaw³

College of Engineering, Swansea University, Swansea, SA1 8EN, UK

M. Amoozgar⁴

School of Computing and Engineering, University of Huddersfield, Huddersfield, HD1 3DH, UK

M.I. Friswell⁵

College of Engineering, Swansea University, Swansea, SA1 8EN, UK

B.K.S. Woods⁶

Department of Aerospace Engineering, University Of Bristol, Bristol, Bs8 1tr, UK

A spiral pulley based mechanism is used to passively balance the energy between the morphing structure and actuation system. Applying the energy balancing concept has the potential to improve the performance of the actuation system by reducing the external energy consumption. In the current study, the energy balancing concept is adopted in a morphing design. A conceptual design of the integration is introduced with gears added between the spiral and load pulleys. The stiffness of the morphing structure is measured and a test rig is built to demonstrate the mechanism. Optimisation is performed to find the design parameters of the passive energy balancing mechanism.

I. Nomenclature

SPNS	=	spiral pulley negative stiffness
FishBAC	=	FishBAC Bone Active Camber
r	=	spiral pulley radius
T_d	=	drive torque provided by the pulley
T_l	=	load torque required by the structure
η_e	=	energy conversion efficiency
L_0	=	drive spring pre-extension
k_{drive}	=	drive spring rate
k_{load}	=	structural stiffness

¹ Postdoctoral researcher, College of Engineering, Swansea University.

² Postdoctoral researcher, College of Engineering, Swansea University.

³ Senior lecturer, College of Engineering, Swansea University.

⁴ Senior lecturer, School of Computing and Engineering, University of Huddersfield.

⁵ Professor, College of Engineering, Swansea University.

⁶ Lecturer, Department of Aerospace Engineering, University of Bristol, AIAA member.

II. Introduction

An actuation system is an essential part of any potential morphing rotorcraft concept. The actuation system needs to provide adequate force and stroke output while keeping the weight and cost minimum. The increase of weight and energy consumption caused by the actuation system could negate the morphing benefits and lead to reduced overall performance. Especially, when the shape change comes from the elastic deformation of morphing structures, the actuation system needs to provide the elastic strain energy for the structural deformation during each shape-changing cycle, which will be dissipated as the energy is not recycled in the system.

The problem caused by the high demand of actuation forces and energies can be solved in several ways. Conventional actuation methods, like hydraulic actuation and servo motors are still often applied in morphing [1]. Smart materials, such as shape memory alloys and polymers, and piezoelectric materials [2, 3], can be applied to introduce new design approaches for morphing aircraft and rotorcraft, although they may require high actuation voltage [4] or have a low actuation bandwidth [5, 6]. Optimisation of the morphing structure as well as the actuation layout can be performed to achieve an improved actuation efficiency. For example, the morphing wingtip structure was optimised [7] to reduce the requirement of actuation force. A distributed actuation system was investigated using a multi-discipline optimisation [8]. Bistable /multistable structures may also require less actuation energy as the actuation is only applied to induce the snap-through [9].

Alternatively, an actuation system based on the passive energy balancing concept has the potential to reduce the energy consumption. Rather than simply increasing the output energy from the actuator, the energy is stored in the system to drive the morphing structure. The entire system consists of the actuation mechanism and the morphing structure, and is balanced. The stored energy, which will be given back by the elastic structure, can be cycled in the system, if frictions and non-elastic deformations are neglected. In this paper, the spiral pulley negative stiffness (SPNS) mechanism is applied to balance the Fish Bone Active Camber (FishBAC) morphing concept [10-12]. The spiral pulley has a spooling cable, which is connected to a pre-stretched spring. The rotation of the spiral pulley can release the energy stored in the spring, and deform the morphing structure. Due to the geometric configuration of the spiral pulley and the kinematic tailoring it provides, 'negative' torque of increasing magnitude is generated as rotation increases, which will balance the 'positive' stiffness of the morphing structure [13].

While previous studies have demonstrated this concept in desktop demonstrators [14-16], it has not previously been demonstrated in a true aerodynamic structure. Limited space in the airfoil raises challenges in terms of the design and manufacturing, especially considering the requirement of the accurate spiral geometry to achieve the stiffness cancellation, the large forces in the pulley cables and adequate stroke of the pulley based actuation mechanism. The current study will firstly define the model used in Section III, in which a gear train is added in the actuation mechanism between the spiral pulley and the load pulley. The optimisation setup is introduced in Section IV. Compared to previous studies, more constraints of the actuation mechanism due to the integration are added and the optimisation variables are categorised into different components. Before the optimisation results are discussed in Section VI, the experimental setup and a simplified demonstrator will be introduced in Section V. The results section discusses the influence of different structural stiffnesses on the optimisation results considering the adaptability of the spiral pulley.

III. Model definition

The integration concept is shown in Fig. 1. Figure 1(a) shows the schematic of the FishBAC design driven by servo motors [12]. The torque generated by the servo motors is transferred onto the spine through two tendons attached to the solid trailing edge section.

A prototype of the bidirectional SPNS was developed by Zhang et al. in [14, 16]. Two spiral pulleys are mounted onto one central shaft, and the bidirectional motion can be achieved through the rotation of the pulleys in opposite directions. A NACA23012 airfoil section is chosen for the integration, and the chord and span are 270mm and 250mm respectively. The current approach uses the cable from the load pulley to drive the tendons on the FishBAC directly as shown in Fig. 1(c), which simplifies the mechanism but can still demonstrate the potential of the spiral pulley.

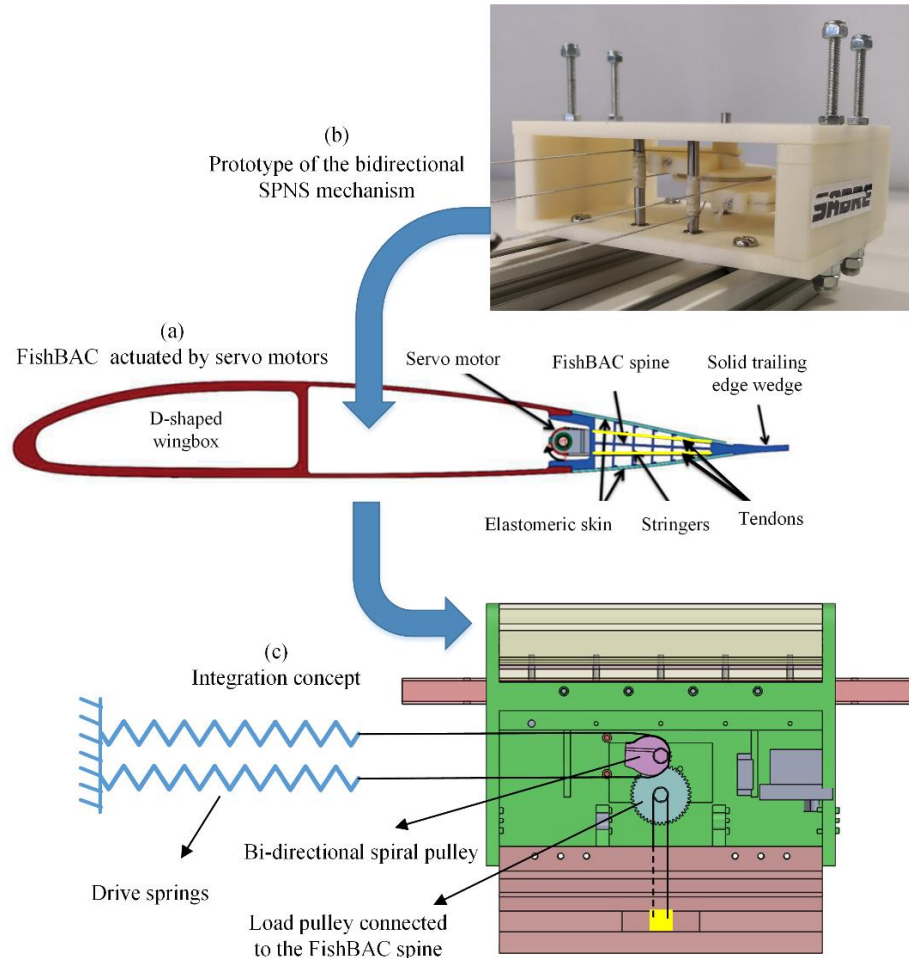


Fig. 1 (a) FishBAC driven by servo motors; (b) Prototype of the bidirectional SPNS mechanism; (c) Integration concept

Figure 2 shows the planar geometry of the spiral pulley and its rotation associated with the drive spring. The radius, r , about point O, which is the centre of the rotation shaft, can be defined as an exponential function

$$r = r_0 + k_1 e^{k_2(\theta + \delta + \delta_0)} \quad (1)$$

where δ is the rotation angle of the spiral pulley and θ is an associated angle. The parameters k_1 , k_2 are the pre-exponent and exponent terms of the spiral pulley. And the coordinate components of point A, x_{off} and y_{off} , are also needed to fully define the pulley geometry, together with the initial pulley radius r_0 and the initial rotation angle δ_0 .

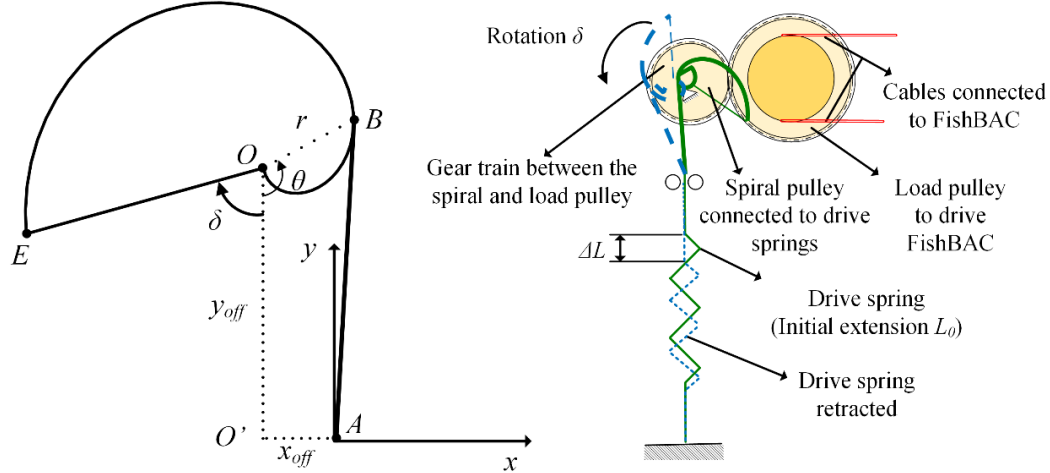


Fig. 2 Geometry of the spiral pulley and its connections to the FishBAC and drive springs

The drive torque output by the load pulley is given by

$$T_d = g \cdot F_d l_m \tag{2}$$

The gear ratio is defined as

$$g = \frac{n_2}{n_1} \tag{3}$$

where the teeth number in the spiral pulley and the load pulley are denoted as n_1 and n_2 respectively.

Figure 3 shows the detailed design of the spiral pulley and the load pulley. The spiral pulley is connected to the pre-stretched springs, which are used to store the energy to balance the FishBAC morphing. A cable is used to connect the spiral pulley and the drive spring. The cable is fixed into an installation hole in the spiral pulley. The load pulley, which will drive the FishBAC, is meshed with the spiral pulley through spur gears. Two cables are used to connect the load pulley and the FishBAC spine.

The expression of the drive torque has been derived in [13, 14]. The force, F_d , is a function of the rotation angle, the parameters of the spiral pulley geometry and the drive spring. The moment arm, l_m , also varies with the rotation of the spiral pulley. And thus, the drive torque is influenced by the geometry parameters of the spiral pulley, the drive spring stiffness and the initial extension. A decreasing torque can be provided against the rotation of the pulley, which leads to the so-called negative stiffness. In the meantime, the load torque, T_l , is required to deform the structure. If the stiffness of the structure can be balanced by the negative stiffness of the spiral pulley mechanism partially or completely, less external energy will be consumed by the actuation system, as the energy stored in the drive spring can help to deform the structure.

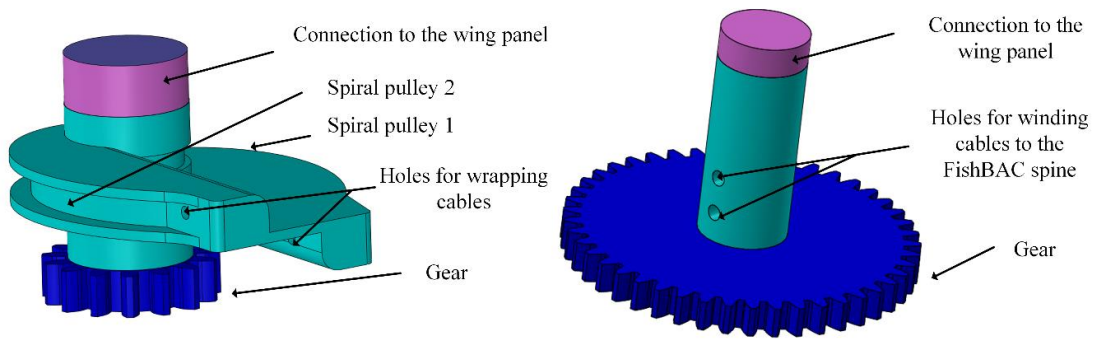


Fig. 3 Schematic of the spiral pulley with detailed designs

When the gear ratio is larger than 1, the drive torque output by the load pulley can be amplified, which can help to overcome high torque requirements. On the other hands, the rotation angle of the spiral pulley will be increased. The rotation range of the load pulley can be limited due to the FishBAC deformation limit, which means only a small fraction of the drive spring pre-extension will be used, and most of the stored energy will not be used to balance the structural deformation. Adding the gear will increase the rotation range of the spiral pulley for the same FishBAC deformation, and increase the efficiency of the passive energy balancing.

IV. Optimisation setup of the spiral pulley

The passive energy balancing device can be sized to improve its performance. The related parameters are listed in Table 1. These parameters can be categorised as component-level parameters, i.e. the parameters of the spiral pulley and the parameters of the drive spring, and the assembly level parameters, i.e. the gear ratio between the spiral and load pulley. Optimisation has been performed in previous research to design the spiral pulley for the single-directional and bi-directional cases [13, 16].

The objective is to find the maximum energy conversion efficiency metric defined as

$$\max \eta_e = \frac{E_o}{E_r} \quad (4)$$

where the energy output by the spiral pulley system, E_o , and the energy required by the FishBAC structure, E_r , can be obtained as

$$E_o = \int_0^{\delta} |T_d| d\delta \quad (5)$$

$$E_r = \int_0^{\delta} |T_l| d\delta$$

The load torque, which is the required torque to deform the structure is denoted as T_l , and is a fixed function of rotation angle determined by the morphing rotorcraft design and will be measured in Section V.

Table. 1 Design parameters in the passive energy balancing device

Parameter name	Parameter level
Initial radius, r_0	component level: spiral pulley geometry parameters
Pre-exponent term, k_1	
Exponent term, k_2	
Initial spiral pulley rotation angle, δ_0	
x-axis offset of the spiral coordinate origin, x_{off}	
y-axis offset of the spiral coordinate origin, y_{off}	
Drive spring pre-extension, L_0	component level: drive spring
Drive spring rate, k_{drive}	
Drive spring initial force, F_0	
Gear ratio between the spiral pulley and the load pulley, g	assembly level

The parameters need to satisfy the constraints, especially when the spiral pulley is integrated into the FishBAC morphing design. Obviously, the straightforward constraint is to ensure the integrated spiral pulley and the load pulley will not have geometry interference within the morphing structure. The space in the morphing rotorcraft is limited and will limit the maximum available size of the spiral pulley.

The geometric constraints are written as

$$\begin{aligned}
r_{\max} &< r_{\text{lim}} \\
N_s r_{\max} + N_l q &< f_c \cdot C \\
\max(h_s, h_l) &< t_c \cdot C
\end{aligned} \tag{6}$$

Here, the maximum radius of the spiral pulley r_{\max} needs to be small enough to avoid any interference with the load pulley, especially considering the rotation of the spiral pulley. The radii of the spiral pulley and load pulley are denoted as r and q . And the coefficients N_s and N_l are used to denote the maximum radii of the pulleys after the gears are added. As the spiral and load pulleys are in the airfoil, the sum of their radii should be smaller than the chord. Also, the height of the spiral and load pulleys, h_s and h_l , should be lower than the airfoil thickness. The chord is denoted as C and two ratios f_c and t_c , are used to represent the chordwise space the pulleys can occupy, and the thickness to chord ratio of the airfoil. It should be noted that the maximum radius of the spiral pulley is constrained by the rotation range of the spiral pulley, as only part of the spiral pulley profile is used.

The maximum stress on the spiral pulley can be found in the connection between the spiral pulley and the cable. A stress concentration will occur and the concentration factor is denoted as K . Since the cable mainly undergoes tensile deformation, the constraint is written as

$$\max K \cdot F < F_{\text{lim}} \tag{7}$$

where the tensile force is denoted as F and the yield force of the cable is denoted as F_{lim} .

V. Experimental setup

As expressed in the optimisation objective, the required torque to deform the morphing structure is required before further integration study. A simple experimental setup is built to find the relationship between the required load torque and the corresponding rotation angle of the load pulley. The experimental setup is shown in Fig. 4. A baseline load pulley is installed, and the cables from the baseline load pulley are bonded to the FishBAC. The baseline pulley is used to transfer the load torque onto the FishBAC structure in the measurement, and is installed at the same location in the FishBAC structure. The torque is applied to the structure using a torque wrench with digital output. And the rotation angle can be seen from the angle gauge connected to the torque wrench. A camera is placed on top of the experimental setup to record the torque and the angle.

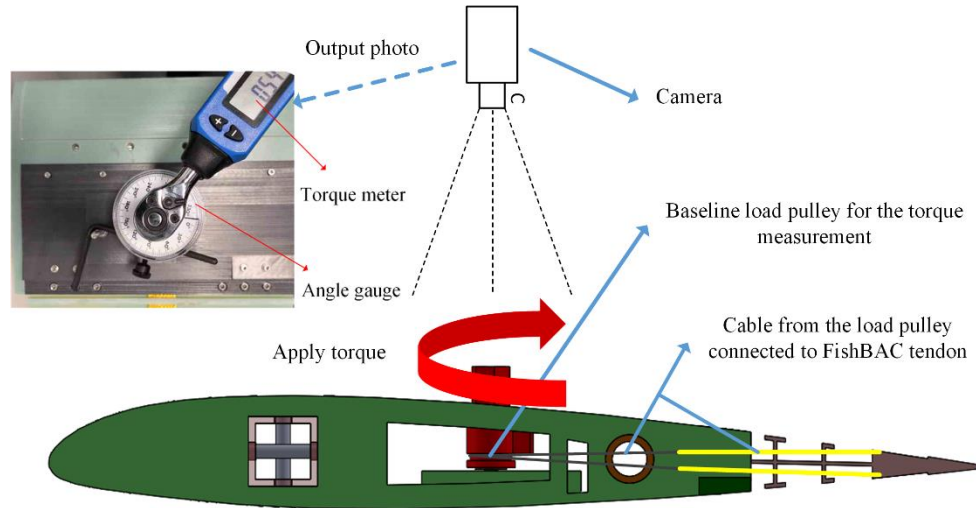


Fig. 4 Schematic of the wing platform for the measurement of the FishBAC structure stiffness

An example of the stiffness test is shown in Fig. 5. Figure 5(a) shows the recorded torque and angle, and the required stiffness to deform the FishBAC downward can be found in Fig. 5(b). The deflections of the FishBAC model are also shown in Fig. 5(c). It was found that the rotation of the load pulley is around 20° and thus the gear ratio is set to 3 to ensure the rotation of the spiral pulley can reach 60° , which can ensure enough displacement of the drive springs.

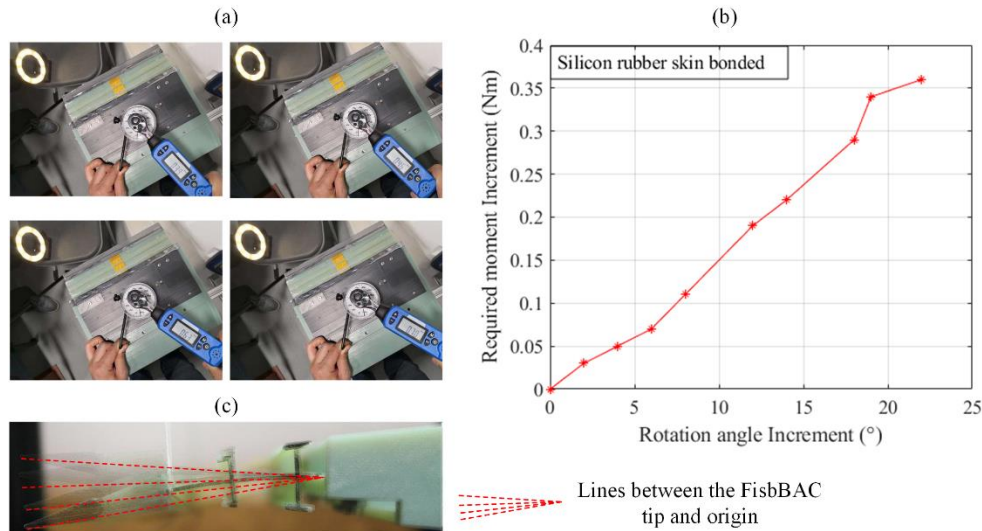


Fig. 5 (a) Record of the torque and the angle change, (b) Required load torque vs the rotation angle of the baseline pulley, (c) Deflections of the FishBAC model

In the integrated morphing rotorcraft, a servo motor will be used in the actuation system. Although the spiral pulley negative stiffness mechanism can reduce the structural stiffness, the actuator is still needed to control the deformation of the FishBAC structure. In theory, the consumed power of the servo motor can be reduced with the help of the spiral pulley mechanism. Before it is applied in the passive energy balancing design, the current characteristic of the servo motor is investigated to show the influence of the load on the servo motor current.

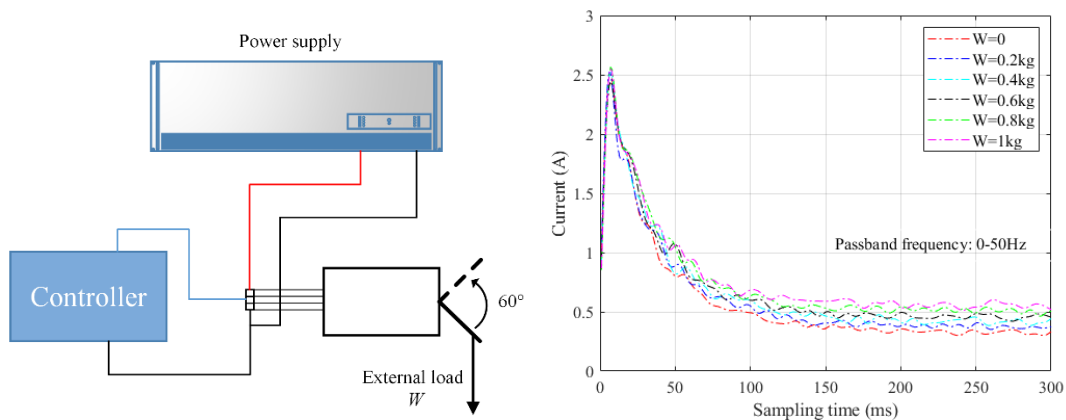


Fig. 6 (a): Setup of the servo motor; (b): Recorded current of the servo motor processed using a low-pass filter with a passband frequency of 50Hz

As shown in Fig. 6, the servo motor is controlled by an Arduino UNO board, and is powered by a DC power supply whose voltage remained at 6V. An external weight is hung onto the servo motor, and the current is recorded by the power supply with the sampling rate equal to 1000Hz. The recorded current is filtered using the MATLAB signal processing toolbox, and the passband frequency is 50Hz. Figure 6 shows a large inrush current occurs when the motor starts to work, but once the motor reaches a steady state, the influence of the external load can be found. Obviously, large external loads will lead to increased currents, which corresponds to large energy consumption.

Figure 7 shows a simplified demonstrator, which is used to verify its mechanism before the passive energy balancing is integrated into the FishBAC morphing rotorcraft. The FishBAC structure is clamped onto a base plate for the convenience of assembling and testing. The demonstrator corresponds to the case when the chord is 270mm and the FishBAC structure accounts for 25% of the chord. The spiral pulley and the load pulley are manufactured using a 3D printer. The drive spring is attached to an aluminum structural rail so that the pre-extension can be adjusted. To

ensure the correct positioning of the spiral pulley origin, the spiral pulley is installed on a base plate with the origin hole drilled, and a top panel is used to provide enough supports to the pulleys.

The optimised spiral pulley parameters from the previous study are used in the simplified demonstrator [16]. The servo motor is used to drive the mechanism and the current in the servo motor is measured using a current sensor. The drive spring stiffness is around 450N/m. the pre-extension is around 0.01m. The servo motor drives the FishBAC structure to deform, and the deflection is around 1.2% of the chord. Due to the large inrush current of the motor, only the current after the motor inrush current is averaged, which is found to be reduced from 1.2A to 1.05A approximately after the spiral pulley mechanism is integrated. The current reduction means 0.375J energy saving for one single operation. Although this energy saving is moderate, the energy reduction can be significant through the entire operation lifetime of the morphing rotorcraft. Clearly, if the load alleviation due to the negative stiffness allows a smaller actuator to be used, there is potential for energy savings at both the steady state and initial region of deployment.

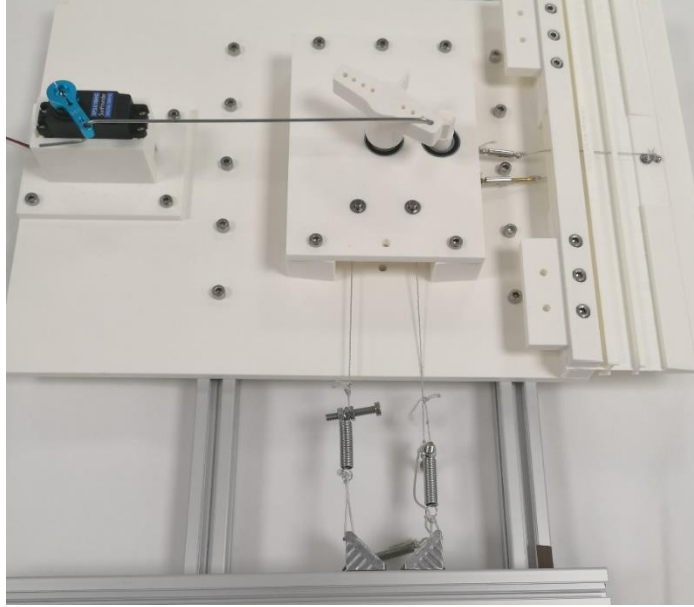


Fig. 7 Simplified demonstrator of the passive energy balancing device

VI. Optimisation results and discussion

The optimisation is performed in MATLAB using genetic algorithm [17]. The structural stiffness measured in Section V is adopted as the design case: $k_{load} = 0.015\text{Nm}/^\circ$. The following variables are optimised within the following ranges:

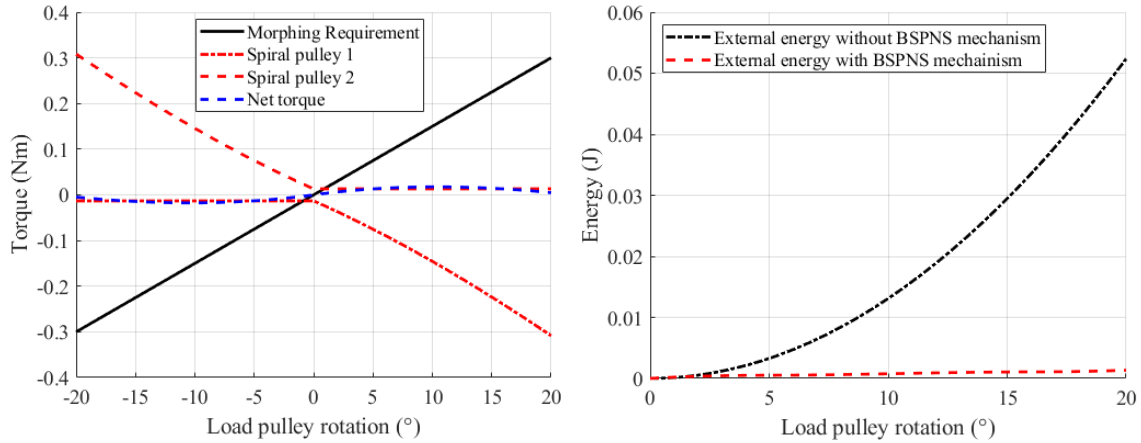
$$\left\{ \begin{array}{l} -30/1000 \leq r_0 \leq 10/1000 \text{ (m)} \\ -0.001 \leq k_1 \leq 0.02 \\ 0 \leq k_2 \leq 1 \\ -50\pi/180 \leq \delta_0 \leq 50\pi/180 \\ -0.1 \leq x_{off} \leq 0.1 \text{ (m)} \\ -0.05 \leq y_{off} \leq 0.1 \text{ (m)} \\ -0.05 \leq L_0 \leq 0.4 \text{ (m)} \\ 100 \leq k_{drive} \leq 1400 \text{ (N/m)} \end{array} \right. \quad (8)$$

The gear ratio is fixed at $g = 3$, and the drive spring initial force $F_0 = 0$ in this case. The geometry and maximum force constraints are not included in the optimisation to allow for a full design space, but are checked after the optimisation. The maximum force in the cable is 25.4 N, which is less than 7% of the yield tensile force of the cable. The optimised variables are listed in Table 2.

Table. 2 Optimised variables in the design case

Parameter name	Optimised value	Unit
Initial radius, r_0	-0.02453	m
Pre-exponent term, k_1	0.01968	-
Exponent term, k_2	0.1968	-
Initial spiral pulley rotation angle, δ_0	-0.1476	rad
x-axis offset of the spiral coordinate origin, x_{off}	-0.04439	m
y-axis offset of the spiral coordinate origin, y_{off}	0.06840	m
Drive spring pre-extension, L_0	0.2944	m
Drive spring rate, k_{drive}	86.3815	N/m

The torque output and the energy efficiency of the spiral pulleys are shown in Fig. 8. The spiral pulley 1 is used for the downward deflection of the FishBAC spine, and the spiral pulley 2 is for the upward deflection, which also corresponds to the positive load pulley rotation. Both the spiral pulleys can eliminate the corresponding required torque, although the other spiral pulley will also cause the residual torque. The net torque of the bidirectional spiral pulley remains close to zero during the entire load pulley rotation. The optimised spiral pulley can reduce the external energy requirement significantly with the help of the energy stored in the pre-stored spring, although the opposite drive spring extension will lead to extra energy requirement.

**Fig. 8 (a) Torque requirements, (b) Energy consumption**

The optimised geometry parameters will generate the profiles of the spiral pulleys, which will be followed by the detailed design. As shown in Fig. 3, there would still be numerous detailed design work of the spiral pulley after obtaining the spiral pulley parameters, especially due to the limited space in the wing. Additionally, the small size and the complex geometry makes the manufacturing of the spiral pulley difficult. 3D printing is applied for the current stage, but the design iteration from the optimisation to the manufacturing is still very time-consuming. The time cost requires the investigation of the adaptability of the spiral pulley mechanism with respect to the variation of the structural stiffness, which corresponds to different load cases caused by the change of the FishBAC structure or the aerodynamic loads.

Figure 9 shows the variation of the external energy when the structural stiffness changes. The x axis corresponds to the structural stiffness, which is normalised by the structural stiffness used in the optimisation case. The y axis corresponds to the ratio between the needed external energy and the required energy to achieve the structural morphing. The optimised case, of which the normalised structural stiffness $k_{load} = 1$, has the minimum external needed energy for morphing. When the normalised structural stiffness is less than 1, external energy will be used to balance the torque generated by the spiral pulley rather than to deform the structure, which represents energy wasted from the overall system. In the extreme case, when the structural stiffness is only 20% of the target design case, over four times of the external energy is required compared to the morphing requirement. When the normalised structural stiffness is higher than 1, more external energy is required to deform the morphing structure. But the ratio between the external energy and the morphing requirement remains below 1, which indicates the external energy is still consumed for structure morphing, rather than for balancing the spiral pulley mechanism.

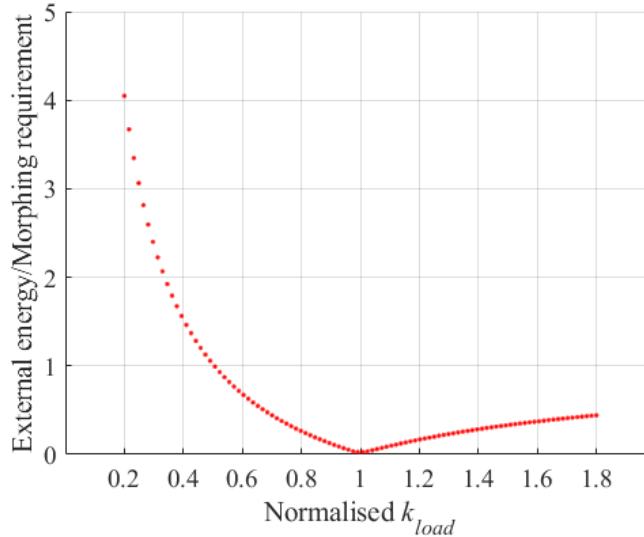


Fig. 9 External energy requirement with the variation of the structural stiffness

The influence of the drive spring parameters is shown in Fig. 10. Both the drive spring stiffness and the pre-extension are optimised at the target design case. Any variation of the drive spring parameters will lead to extra external energy.

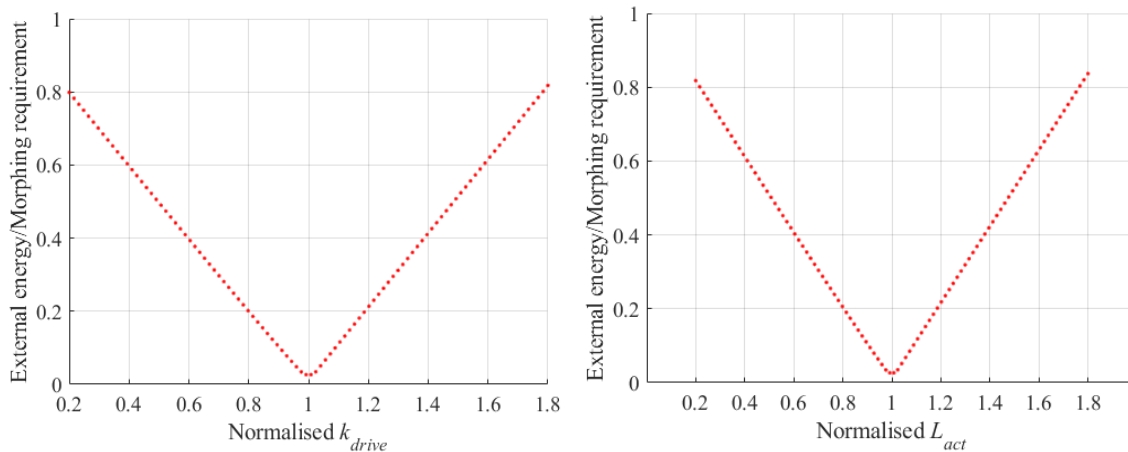


Fig. 10 Influence of the drive spring parameters: (a) k_{drive} , (b) L_{act}

VII. Conclusion

In this paper, passive energy balancing is applied to actuate the FishBAC morphing design. A spiral pulley based mechanism is investigated and integrated into the FishBAC design.

Due to the requirement of optimising the spiral pulley geometry, the load torque, which is required to deform the FishBAC morphing structure, is measured to obtain the structure stiffness. A simplified test rig is built to verify the spiral pulley mechanism. Further optimisation is performed to optimise the parameters of the spiral pulley mechanism.

The optimisation results indicate that the spiral pulley based mechanism is able to provide a negative stiffness against the structural stiffness, which creates an energy balancing system. Parametric analysis also indicates extra energy will be needed if the mechanism does not work at the target design case, or the practical drive spring parameters are not exactly the same to the optimised ones.

The wind tunnel model is under construction, and further results will be obtained to validate the concept.

Acknowledgments

The authors acknowledge the financial support provided by the EU H2020 project SABRE, grant agreement 723491.

References

- [1] Barbarino, S., Bilgen, O., Ajaj, R.M., Friswell, M.I., and Inman, D.J., "A Review of Morphing Aircraft," *Journal of Intelligent Material Systems and Structures*, 2011. Vol. 22, No. 9, 2011, pp. 823-877.
doi: 10.1177/1045389X11414084
- [2] Sun, J., Guan, Q., Liu, Y., and Leng, J., "Morphing Aircraft Based on Smart Materials and Structures: A State-of-the-Art Review," *Journal of Intelligent Material Systems and Structures*, 2016. Vol. 27, No. 17, 2016, pp. 2289-2312.
doi: 10.1177/1045389X16629569
- [3] Li, D., Zhao, S., Da Ronch, A., Xiang, J., Drofelnik, J., Li, Y., Zhang, L., Wu, Y., Kintscher, M., Monner, H.P., Rudenko, A., Guo, S., Yin, W., Kirn, J., Storm, S., and Breuker, R.D., "A Review of Modelling and Analysis of Morphing Wings," *Progress in Aerospace Sciences*, 2018. Vol. 100, No. 2018, pp. 46-62.
doi: 10.1016/j.paerosci.2018.06.002
- [4] Bilgen, O., Kochersberger, K., Diggs, E., Kurdila, A., and Inman, D., "Morphing Wing Micro-Air-Vehicles Via Macro-Fiber-Composite Actuators". *48th AIAA/ASME/ASCE/AHS/ASC Structures, Structural Dynamics, and Materials Conference*, AIAA, Paper 2007-1785, Honolulu, Hawaii. April 23-26, 2007.
doi: 10.2514/6.2007-1785
- [5] Kudva, J.N., Martin, C.A., Scherer, L.B., Jardine, A.P., McGowan, A.R., Lake, R.C., Sendekyj, G., and Sanders, B. *Overview of the DARPA/AFRL/NASA Smart Wing Program. Proc. SPIE 3674, Smart Structures and Materials 1999: Industrial and Commercial Applications of Smart Structures* July 9, 1999.
doi: 10.1117/12.351561
- [6] Kudva, J.N., "Overview of the Darpa Smart Wing Project," *Journal of Intelligent Material Systems and Structures*, 2004. Vol. 15, No. 4, 2004, pp. 261-267.
doi: 10.1177/1045389X04042796
- [7] Wang, C., Haddad Khodaparast, H., Friswell, M.I., Shaw, A.D., Xia, Y., and Walters, P., "Development of a Morphing Wingtip Based on Compliant Structures," *Journal of Intelligent Material Systems and Structures*, 2018. Vol. 29, No. 16, 2018, pp. 3293-3304.
doi: 10.1177/1045389X18783076
- [8] Westfall, J., Canfield, R., Joo, J., and Sanders, B., "Multi-Disciplinary Optimization of a Distributed Actuation System in a Flexible Morphing Wing". *48th AIAA/ASME/ASCE/AHS/ASC Structures, Structural Dynamics, and Materials Conference*, AIAA, Paper 2007-1715, Honolulu, Hawaii. April 23-26, 2007.
doi: 10.2514/6.2007-1715
- [9] Emam, S.A. and Inman, D.J., "A Review on Bistable Composite Laminates for Morphing and Energy Harvesting," *Applied Mechanics Reviews*, 2015. Vol. 67, No. 6, 2015.
doi: 10.1115/1.4032037
- [10] Woods, B.K.S. and Friswell, M.I., "Preliminary Investigation of a Fishbone Active Camber Concept", *ASME 2012 Conference on Smart Materials, Adaptive Structures and Intelligent Systems*. September 19-21, 2012, Stone Mountain, Georgia, USA.
doi: 10.1115/SMASIS2012-8058
- [11] Woods, B.K., Dayyani, I., and Friswell, M.I., "Fluid/Structure-Interaction Analysis of the Fish-Bone-Active-Camber Morphing Concept," *Journal of Aircraft*, 2014. Vol. 52, No. 1, 2014, pp. 307-319.
doi: 10.2514/1.C032725
- [12] Rivero, A.E., Weaver, P.M., Cooper, J.E., and Woods, B.K.S., "Parametric Structural Modelling of Fish Bone Active Camber Morphing Aerofoils," *Journal of Intelligent Material Systems and Structures*, 2018. Vol. 29, No. 9, 2018, pp. 2008-2026.
doi: 10.1177/1045389X18758182
- [13] Woods, B.K. and Friswell, M.I., "Spiral Pulley Negative Stiffness Mechanism for Passive Energy Balancing," *Journal of Intelligent Material Systems and Structures*, 2016. Vol. 27, No. 12, 2016, pp. 1673-1686.
doi: 10.1177/1045389X15600904
- [14] Zhang, J., Shaw, A.D., Mohammadreza, A., Friswell, M.I., and Woods, B.K.S., "Spiral Pulley Negative Stiffness Mechanism for Morphing Aircraft Actuation", *ASME 2018 International Design Engineering Technical Conferences and Computers and Information in Engineering Conference*. August 26-29, 2018, Quebec City, Quebec, Canada.
doi: 10.1115/detc2018-85640
- [15] Zhang, J., Shaw, A.D., Amoozgar, M., Friswell, M.I., and Woods, B.K.S., "Bidirectional Torsional Negative Stiffness Mechanism for Energy Balancing Systems," *Mechanism and Machine Theory*, 2019. Vol. 131, No. 2019, pp. 261-277.
doi: 10.1016/j.mechmachtheory.2018.10.003
- [16] Zhang, J., Shaw, A.D., Mohammadreza, A., Friswell, M.I., and Woods, B.K.S., "Bidirectional Spiral Pulley Negative Stiffness Mechanism for Passive Energy Balancing," *Journal of Mechanism and Robots*, 2019. Vol. 11, No. 5, 2019.
doi: 10.1115/1.4043818
- [17] Mathworks, *Matlab 2019b*, 2019: Natick, MA.